

# Spectral variability in faint high frequency peakers

M. Orienti<sup>1,2\*</sup>, D. Dallacasa<sup>1,2</sup>, C. Stanghellini<sup>2</sup>

<sup>1</sup>*Dipartimento di Astronomia, Università di Bologna, via Ranzani 1, I-40127, Bologna, Italy*

<sup>2</sup>*Istituto di Radioastronomia - INAF, Via P. Gobetti 101, I-40129 Bologna, Italy*

Received 20 November 2018; accepted ?

## ABSTRACT

We present the analysis of simultaneous multi-frequency Very Large Array (VLA) observations of 57 out of 61 sources from the “faint” high frequency peaker (HFP) sample carried out in various epochs. Sloan Digital Sky Survey SDSS data have been used to identify the optical counterpart of each radio source. From the analysis of the multi-epoch spectra we find that 24 sources do not show evidence of spectral variability, while 12 objects do not possess a peaked spectrum anymore at least in one of the observing epochs. Among the remaining 21 sources showing some degree of variability, we find that in 8 objects the spectral properties change consistently with the expectation for a radio source undergoing adiabatic expansion. The comparison between the variability and the optical identification suggests that the majority of radio sources hosted in galaxies likely represent the young radio source population, whereas the majority of those associated with quasars are part of a different population similar to flat-spectrum objects, which possess peaked spectra during short intervals of their life, as found in other samples of high-frequency peaking objects. The analysis of the optical images from the SDSS points out the presence of companions around 6 HFP hosted in galaxies, suggesting that young radio sources resides in groups.

**Key words:** galaxies: active - galaxies: evolution - radio continuum: general - quasars: general

## 1 INTRODUCTION

Our knowledge of the first stages of the evolution of powerful radio sources is based on the study of the population of high frequency peaking radio sources. In the framework of models explaining the evolution of individual radio sources, the spectral peak of young radio sources occurs at high frequencies. Given their small size, in these sources the synchrotron self-absorption (SSA) is a very effective mechanism. As the source grows, the peak frequency is expected to shift towards lower frequencies as a consequence of adiabatic expansion. An alternative explanation suggests that the spectral peak is due to free-free absorption from a ionized medium enshrouding the radio emission (Bicknell et al. 1997). Both scenarios are supported by the empirical anti-correlation found by O’Dea & Baum (1997) from the study of samples of compact steep spectrum (CSS) and gigahertz-peaked spectrum (GPS) radio sources. The former have peak frequencies around a few hundred MHz, typical sizes of a few kpc and ages of  $10^5 - 10^6$  years, whereas the latter have spectra peaking around 1 GHz, typical sizes of about 1 kpc or less and ages of  $10^3 - 10^4$  years. However,

it is worth noting that the consistency between the source size and the spectral peak often found in the most compact sources strongly support the synchrotron self-absorption scenario (Orienti & Dallacasa 2008a; Tingay & de Kool 2003).

High frequency peakers (HFP; Dallacasa et al. 2000), with a spectral peak occurring at frequencies above a few GHz, are thus the best candidates to be newly born radio sources, with ages between  $10^2 - 10^3$  years.

The radio properties of HFPs have been derived by the analysis of the “bright” HFP sample (Dallacasa et al. 2000; Tinti et al. 2005; Orienti et al. 2006a, 2007; Orienti & Dallacasa 2008b). In particular, from the multi-epoch analysis of their radio spectra it has been found that the sample is composed of two different populations. One population consists of radio sources that maintain the convex spectrum without showing variability, whereas the other comprises radio sources that change their spectral shape, becoming also flat-spectrum objects, and possessing substantial flux density variability. The different spectral properties shown by the two populations suggest that the former represent young radio sources still in an early stage of their evolution, while the latter are beamed objects. The analysis of the multi-epoch spectral behaviour has

\* E-mail: orienti@ira.inaf.it

**Table 1.** VLA observations and configurations

Date	Conf	Proj.ID	Code
Sep. 2003	AnB	AD488	a
Jan. 2004	BnC	AD494	b
Nov. 2006	C	AO210	c
Apr. 2007	D	AO210	d

proved to be a powerful tool to discriminate between the two populations (Tornaiainen et al. 2005; Tinti et al. 2005; Orienti et al. 2007). In fact, beamed radio sources, although usually characterized by a flat and variable spectrum, may be selected in samples of high-frequency peaking objects when their emission is dominated by a flaring knot in a jet. On the other hand, young radio sources are known to be the least variable class of extragalactic radio sources (O’Dea 1998). However, it must be mentioned that in the youngest objects, substantial variability in the optically-thick part of the spectrum is expected as a consequence of either the source growth/evolution (e.g. J1459+3337, Orienti & Dallacasa 2008c), or changes in the possible absorber screen, or a combination of both (Tingay & de Kool 2003).

In this paper we present a multi-epoch analysis based on simultaneous multi-frequency VLA data of the radio spectra of 57 high frequency peakers from the “faint” HFP sample (Stanghellini et al. 2009). This sample was selected as the “bright” HFP sample (Dallacasa et al. 2000) by cross-correlating the 87GB survey at 4.9 GHz with the NVSS at 1.4 GHz, and including only sources fainter than 300 mJy at 4.9 GHz within a restricted area around the northern galactic cap (for details on the sample see Stanghellini et al. 2009). The study of the radio properties of a sample of faint HFPs is the first step in understanding the first stages of the radio source evolution. So far, spectral studies have been carried out for the bright HFP sources only, and an extension to fainter objects is necessary. The evolution models developed so far (e.g. Fanti et al. 1995; Snellen et al. 2000; Kaiser & Alexander 1997) predict that in the earliest stage the radio luminosity progressively increases, implying that the youngest objects are likely to be found among faint sources. Furthermore, in faint HFPs, boosting effects should be less relevant, making the contamination from blazars less severe than what found in samples of brighter objects.

Throughout this paper we assume the following cosmology:  $H_0 = 71 \text{ km s}^{-1} \text{ Mpc}^{-1}$ ,  $\Omega_M = 0.27$ , and  $\Omega_\Lambda = 0.73$  in a flat Universe. The spectral index is defined as  $S(\nu) \propto \nu^{-\alpha}$ .

## 2 VLA OBSERVATIONS AND DATA REDUCTION

Simultaneous multi-frequency VLA observations of 57 out of the 61 sources from the “faint” HFP sample

(Stanghellini et al. 2009) were carried out during different runs between September 2003 and April 2007 (Table 1). Observations were performed in L band (with the two IFs centered at 1.415 and 1.665 GHz), C band (with the two IFs centered at 4.565 and 4.935 GHz), X band (with the two IFs centered at 8.085 and 8.465 GHz), U band (14.940 GHz), K band (22.460 GHz), and in Q band (43.340 GHz). At each frequency, the target sources were observed for about 1 minute, cycling through frequencies. During each run, the primary flux density calibrator either 3C 286 or 3C 48 was observed for about 3 minutes at each frequency. Secondary calibrators were chosen on the basis of their distance from the targets in order to minimize the telescope slewing time, and they were observed for 1.5 min at each frequency, every 20 min.

The data reduction was carried out following the standard procedures for the VLA implemented in the NRAO AIPS package. The flux density at each frequency was measured on the final image produced after a few phase-only self-calibration iterations. In the L band it was generally necessary to image a few confusing sources falling within the primary beam. All the target sources appeared unresolved at any frequency. During the observations of a few sources, strong RFI at 1.420 and 1.665 GHz was present, and in those cases the measurements of the flux density were not possible.

Uncertainties on the determination of the absolute flux density scale are dominated by amplitude errors. Based on the variations of antenna complex gains during the various observations, we can conservatively estimate an uncertainty of  $\sim 3\%$  in L, C, and X bands,  $\sim 5\%$  in U band, and  $\sim 10\%$  in K and Q bands. The rms noise level on the image plane is about 0.1 mJy/beam in C and X bands, and about 0.2-0.4 mJy/beam in L, U, and K bands. In the Q band it accounts for 0.4-0.5 mJy/beam, becoming comparable to the amplitude calibration errors for sources fainter than  $\sim 20$  mJy. Results are presented in Section 4.

## 3 OPTICAL DATA

To determine the optical properties of the sources in the faint HFP sample, we complemented the information available in the literature with that provided by the SDSS DR7 (Abazajian et al. 2009). The optical properties of each object (like source extension and magnitude) have been carefully inspected beyond the automated procedures in the SDSS, in order to unambiguously identify the host (i.e. quasar, galaxy, or empty field) of each radio source.

Of the 57 sources considered in this paper, 12 are identified with galaxies with redshift between 0.03 and 0.6; 33 are quasars with a higher redshift, typically in the range from 0.6 to 3.0, while 12 sources still lack an optical counterpart (labelled as empty field (EF) in Table 3).

Images and optical information have been retrieved by means of the SDSS DR7 Finding Chart Tool. In Table 3 we report the R magnitude, converted in the Johnson-Kron-Cousins BVRI system, and the spectroscopic redshift when available. An “f” indicates a photometric redshift.

In Fig. 1 we present the optical images from the SDSS DR7 (Abazajian et al. 2009) of the sources hosted in galaxies.

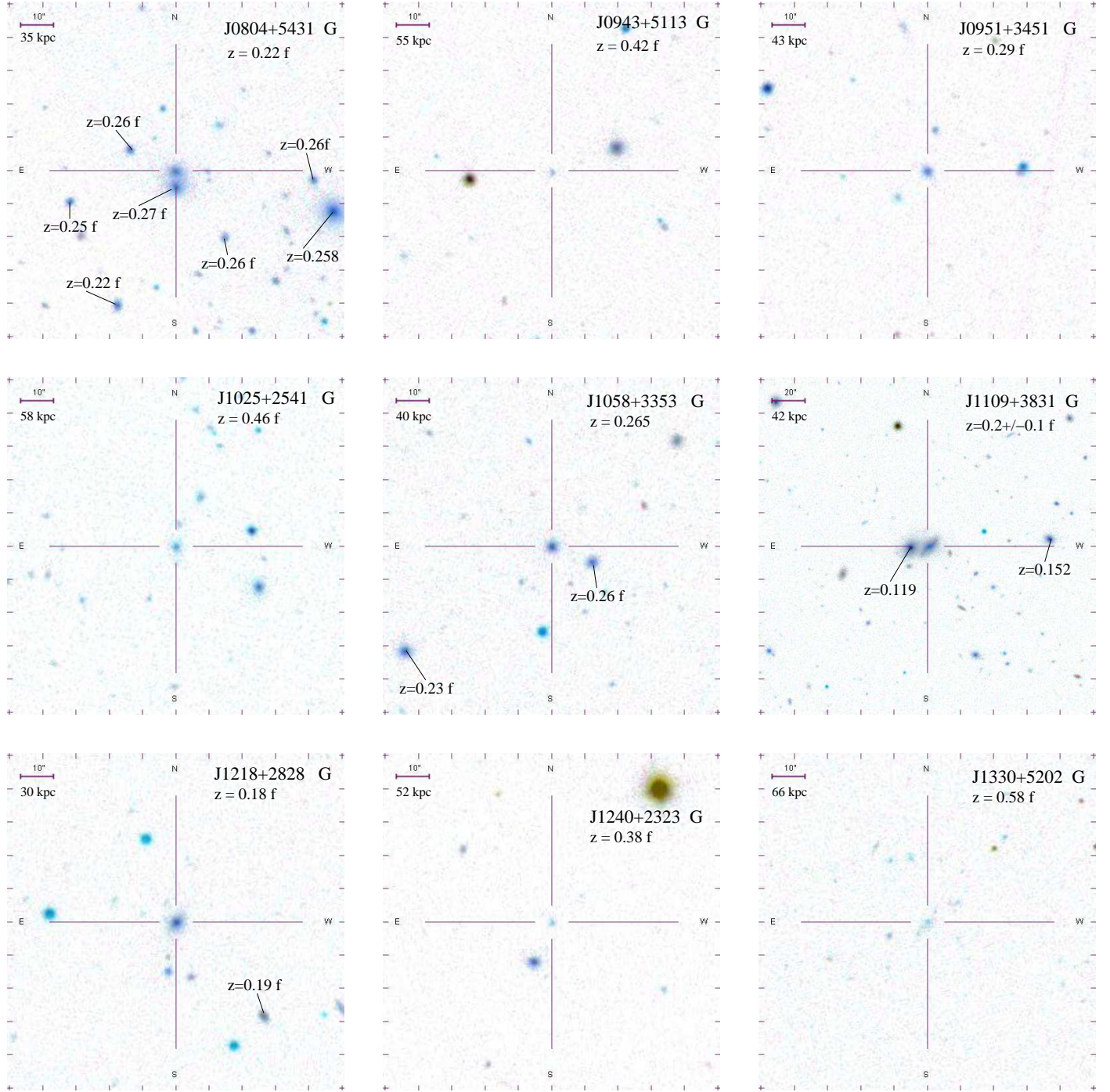


**Figure 1.** Optical images from the SDSS DR7 of the 12 HFP radio sources identified with a galaxy. On the images we report the source name, the redshift (an “f” indicates a photometric redshift). If the source forms a group, we report the redshift of the companion galaxies, when available. The field width has been chosen to show a region of about 250 kpc around the galaxy hosting the HFP radio source.

For the 3 galaxies with available spectroscopic data we show the spectrum in Fig. 2 and we summarize the information on the main lines in Table 2.

### 3.1 Optical properties

A characteristic arising from Fig. 1 is the presence of companions within a projected distance of about 150 - 200 kpc around 6 HFP galaxies. Although in J0804+5431, J1058+3353, J1109+3831, and J1218+2828 this evidence comes from photometric information only, in the case of

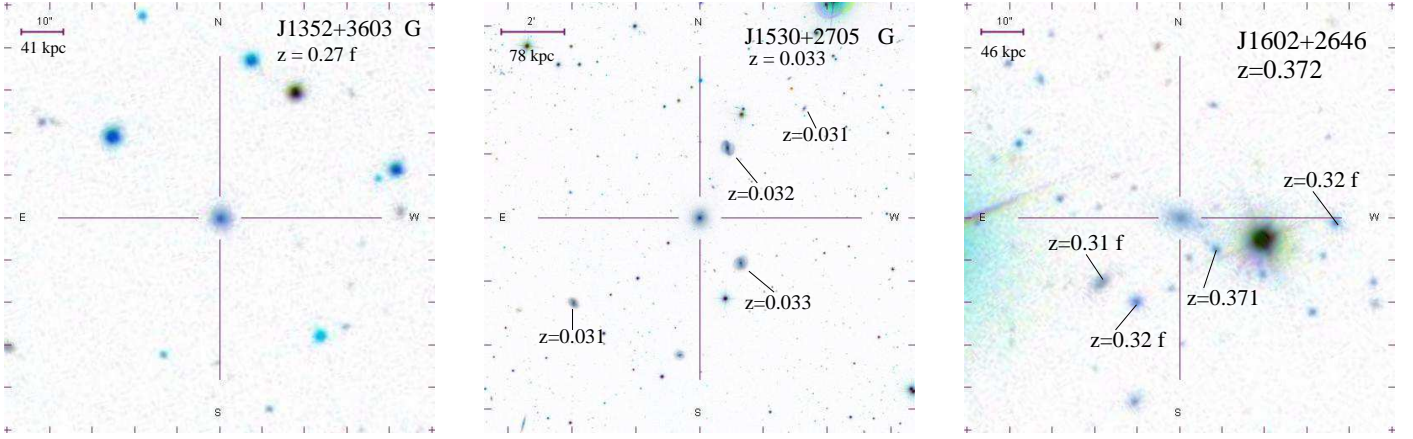


Figure 1. Continued.

J1530+2705 and J1602+2646 the association is confirmed by spectroscopic redshifts, supporting the idea that young radio sources reside in groups, as found in other works (Orienti et al. 2006b; Snellen et al. 2002; Stanghellini et al. 1993). The relatively small redshift of J1530+2705 allows us to identify the spiral morphology of the brightest companions where also a bar is clearly visible.

The galaxies hosting the HFPs are usually the brightest elliptical at the group centre. In the case of J0804+5431 the radio source is hosted by an elliptical galaxy that is at a projected distance of about 160 kpc to the north-east from the brightest galaxy at the centre of the group and it is at a projected distance of about 20 kpc to the north of another elliptical.

An intriguing case is represented by J1109+3831 whose hosting galaxy is a spiral that is located at a projected distance of about 20 kpc from an elliptical. A possible identification error between optical and radio images has been excluded by the analysis of the optical spectrum of the companion, which lacks the typical lines displayed by active galaxies.

Among the HFPs identified with galaxies, 3 objects (J1058+3353, J1530+2705, and J1602+2646) have an optical spectrum in the SDSS DR7. For J1602+2646, the optical spectrum seems to be well fitted by a QSO template, since a large fraction of the light comes from the nuclear region. However, both Fig. 1 and the analysis of the diagnostics  $O[II]/H_{\beta}$  -  $O[III]/H_{\beta}$  clearly indicate that this source is hosted in a galaxy.

The emission lines detected in these objects (Table 2) are those typical for radio galaxies, showing  $[O II] \lambda 3727$ ,  $[O III] \lambda \lambda 4959, 5007$ ,  $H_{\alpha}/N II$ ,  $H_{\beta}$  lines, and  $[O I] \lambda 6300$  in J1058+3353 and in J1602+2646. The  $[O II]/[O III]$  line ratios indicate low ionization, as also found in the optical spectra of faint GPS sources (Snellen et al. 1999).

In the spectrum of each galaxy, the absorption lines associated with stellar populations (4300-Å G band, 5175-Å Mg, and 5900-Å Na D) are clearly visible (Fig. 2), in particular in J1530+2705, where the relatively small redshift allows the

detection of the Ca II lines. The spectra of the companion galaxies (not shown here) have absorption features similar to those found in the HFPs, but without prominent  $[O II]$ ,  $[O III]$ , and  $H_{\beta}$  emission lines, as expected in non-active objects.

To check whether the galaxies of the faint HFP sample follow the Hubble relation found by Snellen et al. (1996), we added the 12 galaxies with spectroscopic and photometric redshift in the GPS R-band Hubble diagram of Snellen et al. (2002). The Hubble diagram, where the HFP galaxies (*squares*) have been added to the GPS galaxies (*crosses*) from Snellen et al. (2002), is presented in Fig. 3, and it indicates that HFP galaxies have a tight distribution in the apparent magnitude-redshift relation, as also found in GPS galaxies (Snellen et al. 1996, 2002).

## 4 RESULTS

### 4.1 Spectral properties

Simultaneous multi-frequency observations carried out at different epochs are necessary to monitor the spectral behaviour and variability of high-frequency peaking radio sources. Variations in the spectral properties, like peak frequency, spectral shape and flux density, are strong indicators of the true nature of the source (Orienti et al. 2007; Tingay & de Kool 2003). In young radio sources the spectral properties are not expected to change, while spectral variability is a typical characteristic of beamed radio sources. To determine a possible variation of the spectral peak, for each source we fitted the simultaneous radio spectrum at each epoch with a pure analytical function:

$$\text{Log} S = a + \text{Log} \nu \cdot (b + c \text{Log} \nu)$$

where  $S$  is the flux density,  $\nu$  the frequency, and  $a$ ,  $b$  and  $c$  are numeric parameters without any direct physical meaning. We prefer to adopt this function instead of that used by Stanghellini et al. (2009) because it better

**Table 2.** Spectral lines of the HFP galaxies with available optical spectrum from the SDSS DR7. Column 1: source name (J2000); Col. 2: line; Col. 3: line frequency in the observer’s frame; Col. 4: line flux density in the observer’s frame; Col. 5: equivalent width in the rest frame.

Source	Line	$\lambda_{\text{obs}}$ Å	$S_{\text{line,obs}}$ $10^{-16} \text{ erg s}^{-1} \text{ cm}^{-2}$	$\text{EW}_{\text{rest}}$ Å
J1058+3353	[O I]	7915.6±1.0	2.1±0.9	5.4±0.7
	[O II]	4713.7±5.3	6.3±1.0	10.0±0.7
	[O III]	6273.6±0.8	0.9±0.3	3.2±0.4
	[O III]	6334.2±0.3	9.9±1.0	10.0±0.4
	H $\beta$	6149.1±0.9	2.0±0.4	5.8±0.5
	H $\alpha$	8304.2±6.2	34.3±1.0	26.0±0.8
J1530+2705	[O I]	6507.5±0.6	0.5±0.1	0.6±0.1
	[O II]	3848.3±4.1	18.3±3.3	5.5±0.3
	[O III]	5120.8±5.1	1.1±0.2	1.6±0.2
	[O III]	5171.2±0.1	6.9±0.7	2.2±0.1
	H $\alpha$	6779.5±5.0	6.8±0.3	2.3±0.1
J1602+2646	[O I]	8643.8±2.4	24.7±5.2	26.4±2.6
	[O II]	5111.8±0.4	239.7±15.8	115.6±2.9
	[O III]	6800.7±0.8	4.7±0.7	13.2±0.9
	[O III]	6865.6±0.5	23.5±2.1	29.6±1.1
	H $\beta$	6669.1±0.3	19.0±1.6	21.9±0.8
	H $\alpha$	9004.7±22.5	519.6±10.5	164.7±3.3

represents the data, providing more accurate values for the peak parameters. The best fits to the spectra are shown in Fig. 4, and the derived peak frequencies at the various epochs are reported in Table 4. Statistical errors derived from the fit are not representative of the real uncertainty on the estimate of the peak frequency. For this reason we prefer to assume a conservative uncertainty on the peak frequency of 10%. The position of the spectral peak is well constrained when the peak occurs at a frequency well sampled by the observations, becoming less accurate when the frequency coverage is not as appropriate. For example, in the case a source has a spectrum peaking at the edges of the frequency coverage (i.e. L or K/Q bands), the fit provides parameters that are less constrained than in the case of sources with the spectral peak occurring around 5-10 GHz, where both the optically thin and thick emission are properly sampled. Spectra poorly constrained are also those lacking observations at some frequencies, as in the case of J1044+4328, J1052+3355, and J1547+3518 where the lack of data either at 1.4/1.7 or 15.3 GHz precluded a reliable determination of their peak frequencies.

By comparing the distribution of the peak frequency of all the sources at the various epochs, we do not find remarkable differences; the changes are usually within the uncertainties. The median value of the peak frequency of the whole sample at each epoch has not changed significantly:  $\nu_p = 5.8$  GHz in the 1998-1999 epoch (namely the observations of the HFP candidates that have been used for selecting the faint HFP sample; Stanghellini et al. 2009);  $\nu_p = 6.2$  GHz in the 2003-2004 epoch; and  $\nu_p = 5.4$  GHz in the 2006-2007 epoch. Among the sources studied here, a few cases show significant variation: in 7 sources (J1053+4610, J1058+3353, J1203+4803, J1251+4317, J1258+2820, J1300+4352, and J1616+4632) the peak measured in the most recent epoch has substantially shifted towards either higher or lower

frequencies. This result indicates that these sources are part of the blazar population, since in young radio sources the shift of the peak towards lower frequencies is not expected to be so remarkable at least on this short time scale (see Section 5).

We computed the spectral index both below ( $\alpha_b$ ) and above ( $\alpha_a$ ) the peak frequency, by fitting a straight line in the optically-thick and -thin part of the spectrum, respectively, following the approach by Tornaiainen et al. (2005) and Orienti et al. (2007). We considered “flat” those sources with both  $\alpha_b > -0.5$  and  $\alpha_a < 0.5$ . In a few sources, depending on the peak frequency, we could fit either  $\alpha_b$  or  $\alpha_a$  only, in order to avoid the flattening near the peak. We find that 12 sources (2 galaxies, 9 quasars, and 1 empty field) show a flat spectrum during at least one of the observing epochs, implying that they are part of the blazar population. The fitted optically thick and thin spectral indices are reported in Table 3.

A case that is worth discussion in detail is the quasar J1008+2533. The radio spectrum shown by this source during two of the observing runs presented here turned out to be a composition of two different spectra: convex at frequencies below 8.4 GHz, and inverted at higher frequencies (see Fig. 4). This shape is similar to that shown by the bright HFP J0927+3902. In J0927+3902 the two-component spectrum is explained by its core-jet structure (see e.g. Orienti et al. 2006a): at frequencies below 1 GHz the spectrum is dominated by the emission from the jet, while at higher frequencies the contribution from the self-absorbed core becomes more important, becoming the dominant emission above  $\sim 10$  GHz. Such a scenario is well supported by pc-scale morphological information by multi-frequency VLBI data (Alberdi et al. 2000). A similar explanation may apply to the case of the faint HFP J1008+2533. Another possibility is that in our new epochs

**Table 3.** Multi-frequency VLA flux density of 57 sources from the faint HFP sample. Column 1: source name (J2000); Col. 2: optical identification from the SDSS DR7: G=galaxy, Q=quasar; EF=empty field; Col. 3: R magnitude; Col. 4: redshift. An “f” indicates a photometric redshift from the SDSS DR7; Col. 5: the observing code from Table 1; Cols. 6 - 14: flux density at 1.4, 1.7, 4.5, 5.0, 8.1, 8.4, 15.3, 22.2, and 43.2 GHz respectively; Cols. 15 and 16: the spectral index computed below and above the spectral peak, respectively.

Source	ID	mag R	z	code	$S_{1.4}$ mJy	$S_{1.7}$ mJy	$S_{4.5}$ mJy	$S_{5.0}$ mJy	$S_{8.1}$ mJy	$S_{8.4}$ mJy	$S_{15.3}$ mJy	$S_{22.2}$ mJy	$S_{43.2}$ mJy	$\alpha_b$	$\alpha_a$
(1)	(2)	(3)	(4)	(5)	(6)	(7)	(8)	(9)	(10)	(11)	(12)	(13)	(14)	(15)	(16)
J0736+4744	Q	20.3	-	b	39	45	60	60	49	47	29	18	9	-0.3	0.8
				c	30	-	53	54	46	48	-	19	-	-0.5	0.7
J0754+3033	Q	17.3	0.769	a	69	77	170	173	182	180	151	130	-	-0.6	0.3
				b	65	70	161	165	174	173	150	116	76	-0.6	0.4
				c	-	-	150	154	166	166	-	95	-	-	0.6
J0804+5431	G	18.1	0.22f	c	37	-	82	81	73	72	-	37	-	-0.7	0.4
J0819+3823	Q	21.6	-	a	18	25	115	120	101	96	48	17	-	-1.4	1.3
				b	16	23	113	116	97	93	45	25	10	-1.6	1.0
				c	14	-	120	127	115	112	-	26	-	-1.7	1.1
J0821+3107	Q	16.9	2.625	c	93	-	95	92	75	74	-	31	-	-	0.7
J0905+3742	EF	-	-	a	54	64	102	100	72	68	29	11	-	-0.5	1.3
				b	51	74	102	99	71	68	35	18	8	-0.6	1.1
J0943+5113	G	20.8	0.42f	a	77	90	160	147	69	64	16	9	-	-0.6	1.8
				c	72	-	163	152	79	75	-	17	-	-0.6	1.4
J0951+3451	G	19.2	0.29f	a	19	29	62	62	56	55	37	26	-	-1.0	0.6
				c	23	-	63	64	59	58	-	24	-	-0.8	0.6
J0955+3335	Q	17.3	2.491	a	45	58	104	106	95	92	60	36	-	-0.6	0.7
				c	49	-	94	94	79	76	-	29	-	-0.5	0.8
J1002+5701	EF	-	-	a	28	39	130	129	72	65	15	-	-	-1.3	1.8
J1004+4328	EF	-	-	b	11	15	36	37	29	29	10	16	10	-1.0	0.6
				c	12	-	36	37	33	32	-	19	-	-1.0	0.4
J1008+2533	Q	18.3	1.960	b	49	66	113	112	100	99	130	161	135	-	-
				c	50	-	116	116	107	108	-	150	-	-	-
J1020+2910	EF	-	-	b	24	27	16	16	15	14	13	10	6	-	0.4
				c	16	-	15	15	14	14	-	7	-	-	0.3
J1020+4320	Q	18.8	1.964	b	118	157	253	247	191	183	116	80	31	-0.6	0.7
J1025+2541	G	19.7	0.46f	b	24	35	47	47	30	29	13	9	5	-0.6	1.0
J1035+4230	Q	19.1	2.440	b	28	28	90	95	98	96	68	44	14	-0.7	0.7
J1037+3646	EF	-	-	b	70	94	146	141	99	94	55	33	11	-0.6	0.9
J1044+2959	Q	18.9	2.983	b	-	-	144	177	163	159	120	96	65	-	0.6
J1046+2600	EF	-	-	b	13	-	38	38	31	30	15	7	4	-0.8	1.0
J1047+3945	Q	20.0	-	b	41	-	39	39	30	30	20	12	9	-	0.4
J1052+3355	Q	16.9	1.407	b	-	-	38	36	22	20	11	5	5	-	1.2
				c	14	-	35	32	20	18	-	6	-	-0.8	1.1
J1053+4610	EF	-	-	b	11	-	36*	38	42	42	54	59	42	-0.6	-
				c	22	-	39	40	60	62	-	75	-	-0.4	-
J1054+5058	Q	22.0	-	c	12	-	20	21	31	32	-	40	-	-0.4	-
J1058+3353	G	18.5	0.265	a	20	26	39	40	41	42	51	51	-	-0.4	-
J1107+3421	EF	-	-	a	21	32	73	72	52	50	21	6	-	-1.1	1.6
				b	25	38	75	73	52	48	25	14	6	-1.0	1.1
				c	28	-	73	72	51	48	-	9	-	-0.8	1.3
J1109+3831	G	17.7	0.2f	a	12	14	53	59	90	91	77	56	-	-1.1	0.4
				b	13	15	50	55	88	89*	81	59	23	-1.0	0.4
				c	14	-	50	55	95	98	-	53	-	-1.1	0.6
J1135+3624	EF	-	-	a	28	37	58	58	46	45	21	11	-	-0.6	1.0
				c	28	-	59	59	50	49	-	13	-	-0.6	1.0
J1137+3441	Q	18.6	0.835	a	25	34	78	83	85	121	157	169	-	-0.7	-
J1203+4803	Q	16.2	0.817	a	187	-	529	562	721	734	788	761	-	-0.6	-
				c	218	252	416	425	452	458	-	384	-	-0.4	0.2
J1218+2828	G	18.1	0.18f	a	25	28	92	96	98	97	69	58	-	-0.7	0.5
J1239+3705	Q	21.4	-	a	-	-	93	101	129	130	112	86	-	-0.5	0.4
				c	13	17	96	107	145	146	-	100	-	-1.3	0.4

Table 3. Continued

Source	ID	mag R	z	code	$S_{1.4}$ mJy	$S_{1.7}$ mJy	$S_{4.5}$ mJy	$S_{5.0}$ mJy	$S_{8.1}$ mJy	$S_{8.4}$ mJy	$S_{15.3}$ mJy	$S_{22.2}$ mJy	$S_{43.2}$ mJy	$\alpha_b$	$\alpha_a$
(1)	(2)	(3)	(4)	(5)	(6)	(7)	(8)	(9)	(10)	(11)	(12)	(13)	(14)	(15)	(16)
J1240+2323	G	21.0	0.38f	a	27	28	52	53	59	60	54	49	-	-0.6	0.2
				c	24	-	58	60	65	65	-	56	-	-0.6	-
J1240+2425	Q	16.9	0.831	a	78	-	60	58	45	44	32	27	-	-	0.4
				c	57	-	58	56	45	44	-	17	-	-	0.5
J1241+3844	Q	21.5	-	c	20	21	23	25	20	20	-	13	-	-0.2	0.4
J1251+4317	Q	18.7	1.453	a	-	-	54	57	80	82	112	116	-	-0.4	-
				c	25	-	72	80	138	142	-	105	-	-1.0	0.3
J1258+2820	Q	19.2	-	a	25	32	51	52	51	50	43	38	-	-0.6	0.2
				c	23	34	45	45	54	54	-	54	-	-0.3	-
J1300+4352	Q	19.6	-	c	140	155	116	115	97	95	-	81	-	-	0.2
J1309+4047	Q	18.9	2.910	a	37	-	139	131	118	115	76	40	-	-1.1	0.8
				c	34	51	132	133	113	110	-	33	-	-1.1	0.9
J1319+4951	Q	19.1	-	a	25	-	49	49	39	39	25	21	-	-0.5	0.5
				c	22	30	50	49	43	43	-	20	-	-0.7	0.6
J1321+4406	Q	21.2	-	a	62	-	73	74	71	70	58	50	-	-0.1	0.3
				c	65	73	78	77	75	74	-	38	-	-0.1	0.4
J1322+3912	Q	17.5	2.985	a	117	-	227	223	181	176	118	86	-	-0.6	0.6
				c	116	135	200	196	150	146	-	56	-	-0.5	0.8
J1330+5202	G	20.7	0.58f	c	91	103	176	180	180	177	-	156	-	-0.4	0.1
J1336+4735	Q	19.7	-	a	-	-	61	61	52	51	26	22	-	-	0.7
				d	26	-	67	67	57	56	-	30	-	-	0.5
J1352+3603	G	18.0	0.27f	a	65	70	102	103	95	93	65	37	-	-0.4	0.7
				d	59	-	97	97	84	82	-	34	-	-0.4	0.7
J1420+2704	Q	20.3	-	a	14	-	55	57	55	53	34	25	-	-1.1	0.6
				d	14	-	62	63	58	56	-	26	-	-1.2	0.6
J1436+4820	EF	-	-	a	20	-	72	72	61	58	32	13	-	-1.0	1.1
J1459+3337	Q	16.6	0.645	a	22	30	195	221	403	415	470	435	-	-1.3	-
J1530+2705	G	14.1	0.033	a	13	14	43	46	45	43	17	13	-	-1.0	0.8
				d	11	12	48	49	42	41	-	23	-	-1.1	0.5
J1547+3518	Q	21.2	-	a	-	-	53	57	67	67	74	72	-	-0.3	-
				d	12	-	49	51	57	58	-	74	-	-0.6	-
J1602+2647	G	18.4	0.372	a	39	-	131	148	238	244	259	224	-	-0.8	-
J1613+4223	Q	19.8	-	b	42	-	206	201	119	110	39	14	-	-1.4	1.7
				d	40	-	201	194	114	105	-	13	-	-1.4	1.7
J1616+4632	Q	19.3	0.950	d	88	-	141	144	148	147	-	129	-	-0.3	0.1
J1617+3801	Q	19.0	1.607	a	23	-	71	75	99	100	95	67	-	-0.8	0.4
J1624+2748	EF	-	-	a	20	-	109	118	175	177	198	173	-	-1.0	-
J1651+3417	EF	-	-	b	-	-	46	48	58	58	49	22	16	-	0.9
J1702+2643	Q	17.2	-	b	35	39	41	42	49	50	61	65	73	-0.2	-
J1719+4804	Q	15.3	1.084	a	75	-	126	135	158	157	115	85	-	-0.4	0.6
				b	66	-	122	127	150	148	113	73	30	-0.5	0.7
				d	60	-	112	114	100	97	-	43	-	-0.5	0.6

a flare from a self-absorbed knot in the jet occurred, causing an increase of the flux density at high frequencies, as also found in blazar objects. The lack of pc-scale morphology information does not allow us to unambiguously determine the origin of this complex spectrum.

## 4.2 Variability index

Following the approach by Tinti et al. (2005) and Orienti et al. (2007) we investigate the presence of flux density variability, by computing the variability index  $V$ :

$$V = \frac{1}{m} \sum_{i=1}^m \frac{(S_i - \bar{S}_i)^2}{\sigma_i^2} \quad (1)$$

where  $S_i$  is the flux density at the  $i$ -th frequency measured at one epoch,  $\bar{S}_i$  is the mean value of the flux density computed averaging the flux density at the  $i$ -th frequency measured at all the available epochs,  $\sigma_i$  is the rms on  $S_i - \bar{S}_i$ , and  $m$  is the number of sampled frequencies. We prefer to compute the variability index for each new epoch (see Table 4) instead of considering all the epochs together in order to better detect the presence of a possible burst. As in Tinti et al. (2005), we consider variable those sources with a variability index  $V > 9$ .

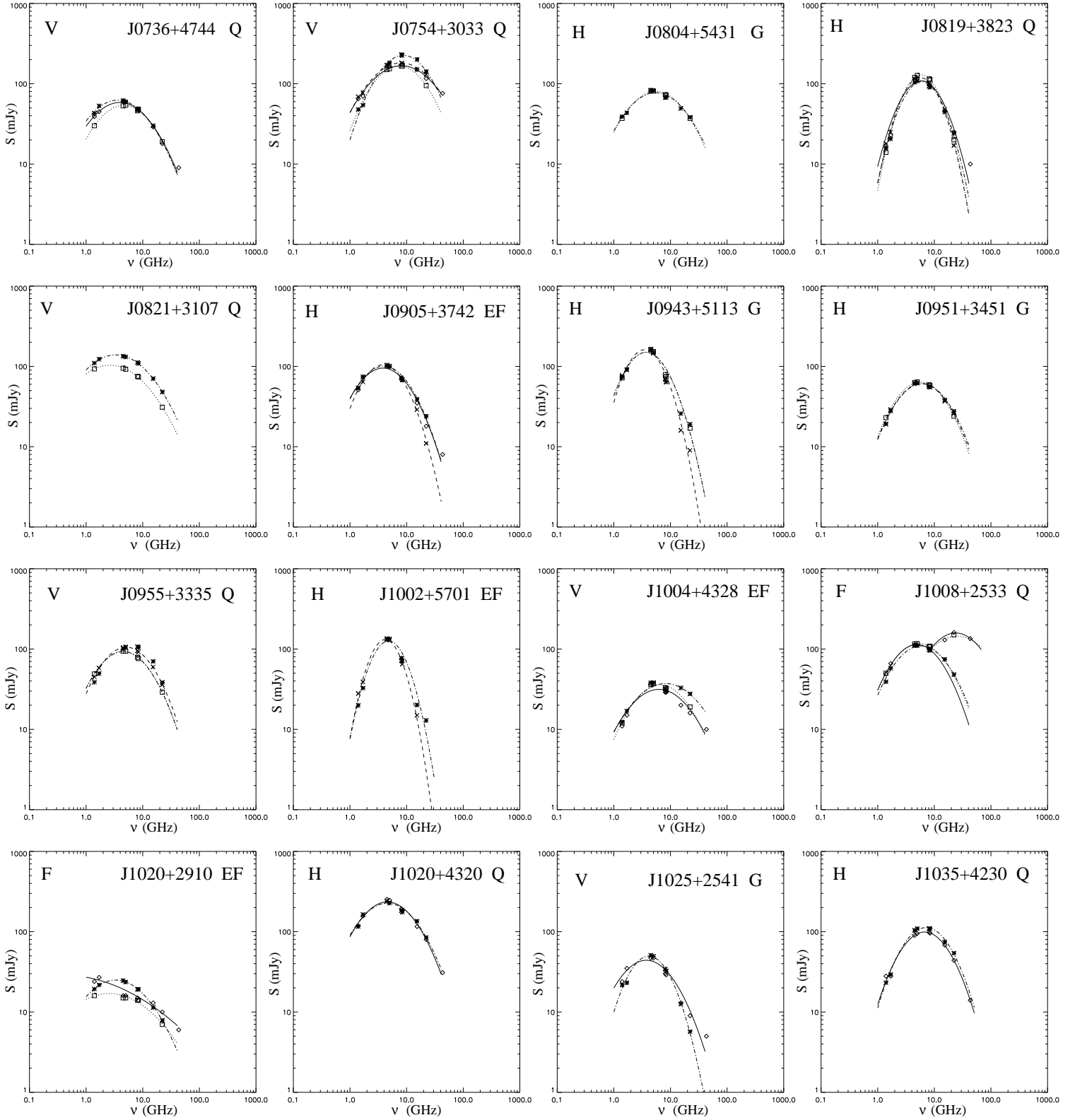


**Figure 4.** Radio spectra of the 57 candidate HFPs from the “faint” HFP sample observed with the VLA during the observing runs presented in this paper. Asterisks and a dash-dotted line refer to the first epoch observations (1998-2000, Stanghellini et al. 2009); crosses and a dashed line refer to epoch  $a$  (2003); diamonds and a solid line refer to epoch  $b$  (2004); squares and a dotted line refer to epochs  $c, d$  (2006-2007).

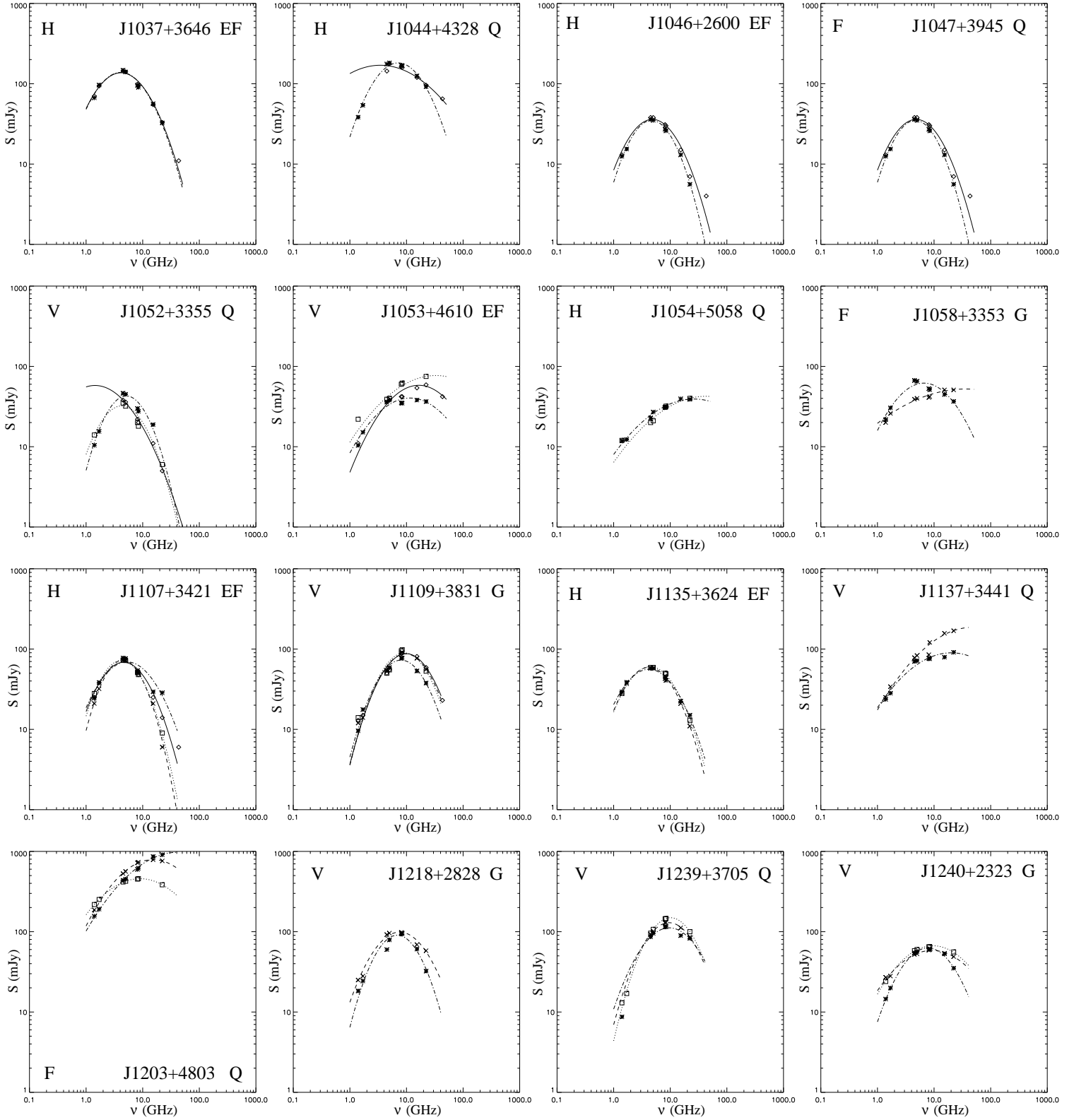


Figure 4. Continued.

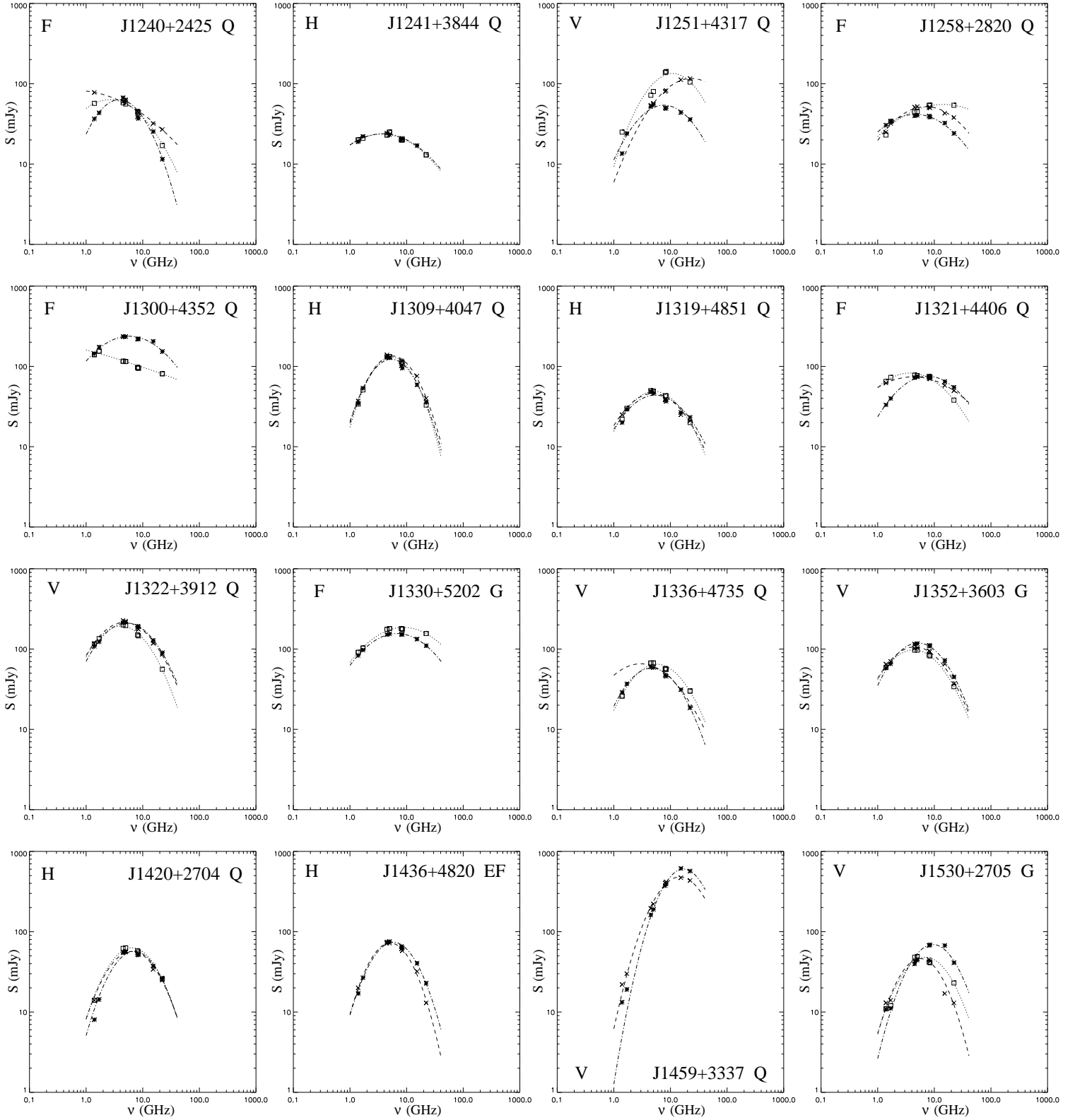


Figure 4. Continued.

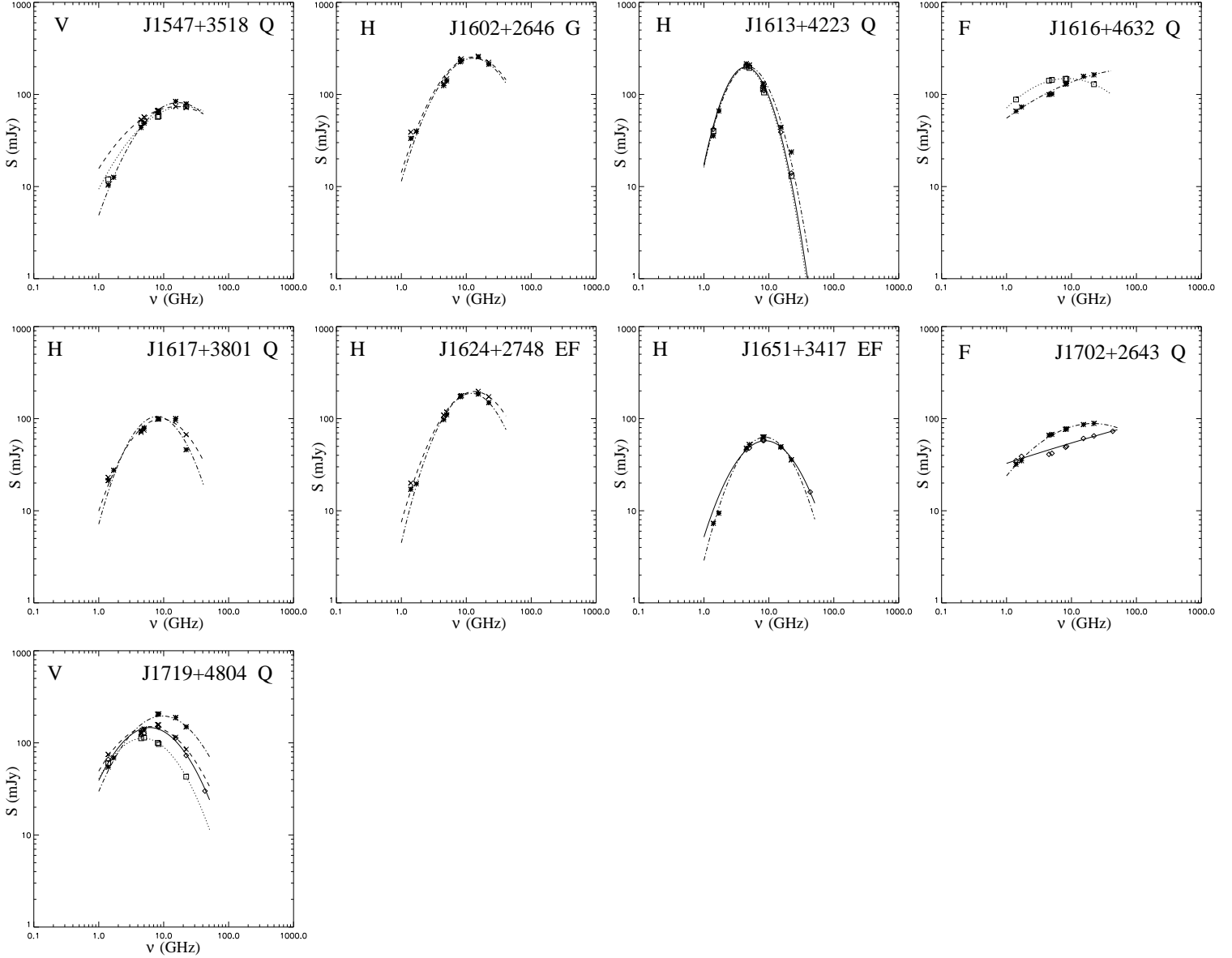


Figure 4. Continued.

From the comparison of the multi-epoch spectral properties and variability we find:

- 24 objects maintain the convex spectrum without showing significant flux density variability ( $V < 9$ ). They are labelled “H” in Column 9 of Table 4;
- 21 sources preserve the convex spectrum at the various epochs, although with some amount of flux density variability ( $V > 9$ ). They are labelled “V” in column 9 of Table 4;
- 12 sources with a convex spectrum in the first epoch (Stanghellini et al. 2009) show a flat spectrum at least in one of the subsequent epochs. They are marked with “F” in Column 9 of Table 4.

### 4.3 Radio properties versus optical identification

The optical identification of the radio sources in samples of CSS and GPS objects (e.g. Fanti et al. 1990; Stanghellini et al. 1998; Snellen et al. 1998; Fanti et al. 2001) showed that in “faint” samples there is a higher fraction of objects identified with galaxies with respect to “bright” samples, and the fraction of galaxies seems to be anti-correlated with the peak frequency, i.e. in CSS samples a higher percentage of radio sources are hosted in galaxies than in GPS and HFP samples. This is easily seen in Fig. 5, where we have plotted the peak frequency versus the peak flux density for the sources from the bright HFP sample (Dallacasa et al. 2000), the faint HFP sample (Stanghellini et al. 2009), the GPS sample (Stanghellini et al. 1998), the faint GPS sample (Snellen et al. 1998); the half-Jansky GPS sam-

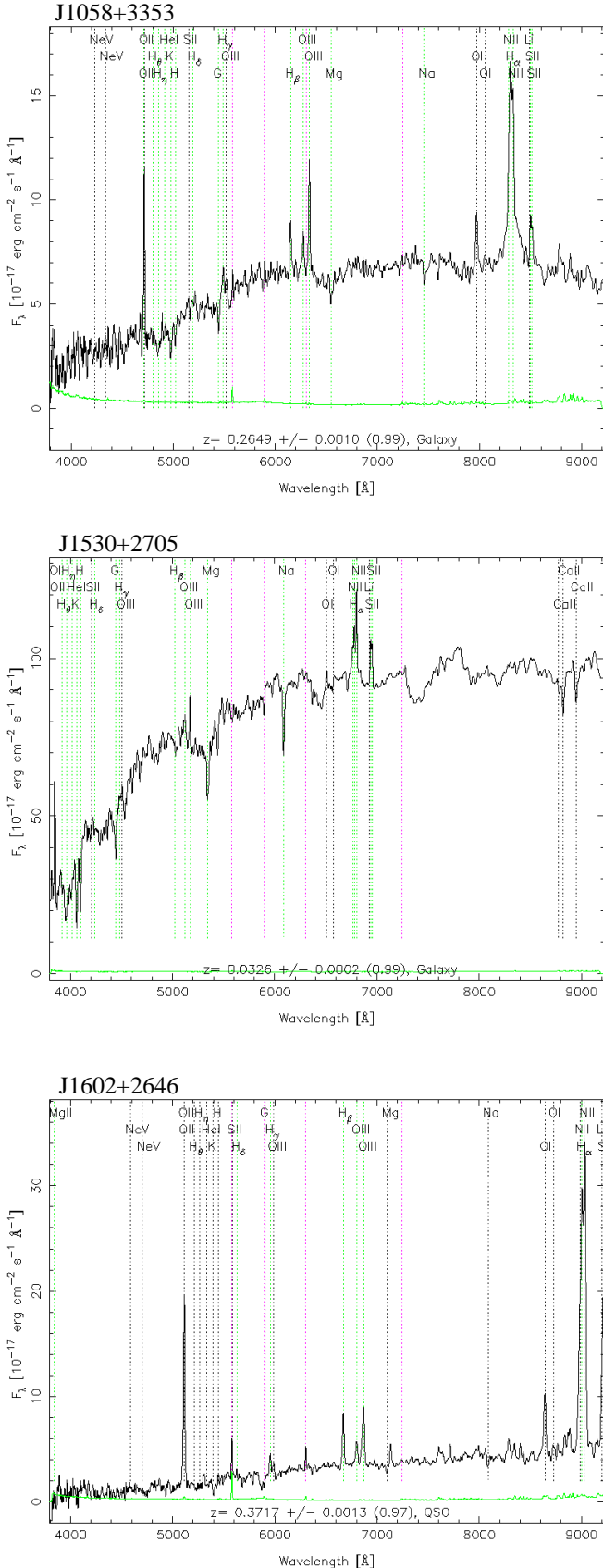


**Figure 2.** Optical spectra from the SDSS DR7 of the galaxies J1058+3353 (*top*), J1530+2705 (*center*), J1602+2642 (*bottom*).

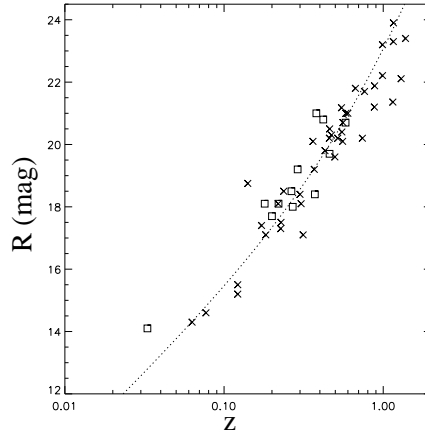


**Figure 3.** The Hubble diagram of HFP galaxies (*squares*) and GPS galaxies (*crosses*, Snellen et al. 2002). The dotted line represents the Hubble relation for GPS galaxies as found by Snellen et al. (1996).

ple (Snellen et al. 2002), and the B3-VLA CSS sample (Fanti et al. 2001). In the latter sample only objects with spectra peaking above 100 MHz have been considered, since for sources with a peak at lower frequency, the turnover frequency could not be reliably constrained. In this plot, radio sources identified with galaxies (*squares*) mainly occupy both the top left part of the panel, i.e. low peak frequency and high peak flux density, and the bottom right panel, i.e. high peak frequency (usually below 10 GHz) but low peak flux density. On the other hand, quasars (*circles*) are mostly found in the left part of the plot, with peak frequencies above a few GHz, and peak flux densities that span almost three orders of magnitude. Radio sources without an optical identification (*triangles*) are found in the same regions as galaxies, suggesting that the majority of these objects share the same properties of the galaxies, but they are fainter probably because they are at higher redshift. It is worth noting that the criteria that have been used to date to select radio source catalogues cannot pick up objects with both low peak frequency and low peak flux density (bottom left panel), indicating that we miss the population of faint CSS objects.

Statistical studies on the correlation between the radio characteristics and the optical counterpart indicate that those objects hosted in a galaxy have the typical properties of young radio sources (i.e. symmetric radio structure and no spectral variability), whereas those identified with quasars are more similar to flat-spectrum radio objects. This suggests that there is a dichotomy between the optical identification and the radio properties: quasars are more likely part of the flat-spectrum blazar population, while galaxies are likely associated with genuinely young radio sources. In the case of the sources from the faint HFP sample studied in this paper, the comparison between their optical identification and the radio variability showed that the majority of quasars have a variable spectrum, while a smaller fraction maintain the convex spectrum without variability (33% H, 39% V, and 28% F). In the case of galaxies, we found that the fraction of variable objects is

still larger than those without spectral variability (34% H, 50% V, and 16% F). For the sources still lacking an optical identification we found that the majority do not show significant spectral variability (75% H, 17% V, 8% F). Among the 12 sources with a flat radio spectrum, we found that two objects (J1058+3353 and J1330+5202) are identified with a galaxy, and one (J1020+2910) lacks an optical identification. When we compare the variability properties of sources with different optical identification by means of the Student's t-statistic we find that there is a significant difference ( $>90\%$ ) between galaxies and quasars, indicating that the majority of galaxies and quasars are associated with different radio source populations.

## 5 DISCUSSION

The anti-correlation found between the projected linear size and the peak frequency (O'Dea & Baum 1997; Bicknell et al. 1997; Snellen et al. 2000) implies that the sources with the spectral peak occurring above a few GHz should represent the population of the smallest radio sources whose radio emission has recently turned on. Samples of high-frequency peaking objects have been selected by choosing sources with an inverted radio spectrum up to 5 GHz (Dallacasa et al. 2000; Tornaiainen et al. 2005; Stanghellini et al. 2009), i.e. the highest observing frequency where a large area survey is presently available. However, due to the selection criteria these samples have been found to comprise both young radio sources and flaring flat-spectrum objects selected during particular phases of their spectral variability, for example when their radio emission is dominated by a knot in the jet. The study of flux density and spectral variability based on repeated simultaneous multi-frequency observations has proved to be an ideal tool in discriminating the different nature of the sources. It was found that in samples of bright objects, where there is a high incidence of sources optically identified with quasars, flat-spectrum blazar objects represent the dominant population (e.g. Tornaiainen et al. 2007; Orienti et al. 2007; Jauncey et al. 2003). A higher incidence of genuinely young radio sources is expected in samples of faint objects where the majority of radio sources should be hosted in galaxies and boosting effects are supposed to play a minor role.

The optical identification of the sources studied in this paper by means of the SDSS DR7 indicates that 21% of objects are hosted in galaxies, i.e. similar to the fraction of galaxies in the bright HFP sample. However, in the faint sample, another 21% of objects lack optical identification and thus a reliable comparison between the two samples cannot be done. The analysis of the optical images of the galaxies hosting HFP pointed out the presence of companions around 6 HFP candidates, indicating that young radio galaxies, like powerful extended radio sources, are in groups, as previously suggested by Stanghellini et al. (1993), indicating a continuity between compact young objects and the population of classical radio galaxies (O'Dea et al. 1996).

Although in 4 galaxies the presence of companions is suggested by photometric information only, in J1530+2705

and J1602+2646 the association is made by spectroscopic redshift. The companion galaxies are located within a projected distance of about 150 - 200 kpc from the target which usually is hosted in the brightest elliptical at the group centre. A peculiar case is represented by J1109+3831, whose parent galaxy seems to be a spiral that is interacting with an elliptical. Young radio sources are normally associated with ellipticals. The case represented by J1109+3831 may be explained by the possible interaction between the hosting spiral and the companion that may have triggered the radio emission. The small redshift of J1530+2705 enabled us to identify the morphology of its brightest companions that turned out to be barred spirals. This group resembles that of the bright HFP J0655+4100 (Orienti et al. 2006b), and in both cases the HFP is hosted by the central elliptical galaxy at the group centre. The presence of companion galaxies in the environment of galaxies hosting young radio sources suggests that the onset of the radio emission may be triggered by merger or interaction events that occurred not long ago. This scenario is supported by the proximity of the companions in J0804+5431 and in J1109+3831, although observations to establish a physical interaction are needed to unambiguously verify this idea.

From the analysis of the multi-epoch radio spectra of the sources in the faint HFP sample, we find a high fraction of objects displaying some level of variability. This result does not imply that all these sources are part of the blazar population. In fact, changes in the radio spectrum may be a direct consequence of the source expansion (e.g. Tingay & de Kool 2003). In newly born radio sources, the evolution timescales can be of the order of a few tens of years. Changes in the radio spectrum of such young objects can be appreciable after the short time (5-8 years) elapsed between the first and last observing run. A clear example is represented by the faint HFP J1459+3337 (Orienti & Dallacasa 2008c). This HFP showed a steadily increasing flux density at 1.4 and 5 GHz, in the optically thick regime, and its spectral peak shifted from 30 GHz down to 12 GHz in about 10 years (Edge et al. 1996). This behaviour is consistent with the flux density and spectral evolution of a young object, with an age of about 50 years, undergoing adiabatic expansion.

In the presence of adiabatic expansion of a homogeneous synchrotron source, the radio spectrum undergoes a shift towards low frequencies. In the optically-thick regime this means that at a given frequency the flux density  $S$  increases with time (see Pacholczyk 1970, Orienti et al. 2007, and Orienti et al. 2008b for a detail analysis of the radio spectrum evolution):

$$S_1 = S_0 \left( \frac{t_0 + \Delta t}{t_0} \right)^3 \quad (2)$$

where  $S_0$  and  $S_1$  are the flux densities at the time  $t_0$  and  $t_0 + \Delta t$ , respectively. On the other hand, the spectral peak  $\nu_p$  moves to lower frequencies:

$$\nu_{p,1} = \nu_{p,0} \left( \frac{t_0}{t_0 + \Delta t} \right)^4 \quad (3)$$

where  $\nu_{p,0}$  and  $\nu_{p,1}$  are the peak frequency at the time  $t_0$  and  $t_0 + \Delta t$  respectively.

**Table 4.** Peak frequency and flux density variability. Column 1: source name (J2000); Col. 2: peak frequency in GHz of the first epoch (1998-2000, Stanghellini et al. 2009); Cols 3, 4, and 5: peak frequency in GHz of epoch *a* (2003), *b* (2004), and *c, d* (2006-2007); Cols. 6, 7, and 8: variability index *V* computed for the epoch *a, b, c, d* respectively; Col. 9: the classification of the source spectrum (*V*=variable, *H*=genuine HFP, *F*=flat; see Section 3). An asterisk indicates that the peak frequency is not reliable due to poor frequency coverage. <sup>1</sup>: for the source J1008+2533 we report the peak of the lowest part of the spectrum.

Source (1)	$\nu_{\text{ep1}}$ (2)	$\nu_{\text{ep2}}$ (3)	$\nu_{\text{ep3}}$ (4)	$\nu_{\text{ep4}}$ (5)	$V_a$ (6)	$V_b$ (7)	$V_{c,d}$ (8)	Var. (9)
J0736+4744	3.6		3.9	4.6	6.3		22.2	V
J0754+3033	8.8	7.9	8.1	7.3	27.5	22.4	19.9	V
J0804+5431	5.4			5.5			2.3	H
J0819+3823	5.8	5.6	6.2	6.1	6.7	3.0	4.0	H
J0821+3107	3.3			2.6			166.6	V
J0905+3742	3.9	3.8	3.7		13.6	1.5		H
J0943+5113	3.7	3.4		3.7	14.7		12.6	H
J0951+3451	6.0	6.1		5.6	1.1		4.3	H
J0955+3335	5.8	5.2		4.5	7.4		57.9	V
J1002+5701	4.6	4.1			14.4			H
J1004+4328	8.0		5.5	6.5		10.3	10.9	V
J1008+2533 <sup>1</sup>	5.8		5.0	5.4		64.6	27.2	F
J1020+2910	3.3		1.5	2.6		14.2	22.5	F
J1020+4320	4.5		4.5			10.9		H
J1025+2541	4.1		3.6			14.3		V
J1035+4230	7.0		6.7			18.2		H
J1037+3646	4.0		4.0			1.0		H
J1044+4328	6.9		3.4*			20.3		H
J1046+2600	4.7		4.3			4.1		H
J1047+3945	3.7		1.6			62.2		F
J1052+3355	5.0		2.3*	4.1		11.0	28.0	V
J1053+4610	11.5		17.6	>22		110.0	352.4	V
J1054+5058	>22			>22			5.3	H
J1058+3353	6.4	>22			71.6			F
J1107+3421	4.6	4.5	5.2	4.2	12.8	0.9	4.0	H
J1109+3831	8.1	9.3	9.2	9.3	5.1	8.4	14.1	V
J1135+3624	4.1	4.2		4.4	0.9		5.5	H
J1137+3441	23.0	>22			146.8			V
J1203+4803	>22	15.2		9.0	600.0		1058.1	F
J1218+2828	7.1	7.5			50.7			V
J1239+3705	9.5	9.5		10.0	23.6		35.2	V
J1240+2323	7.8	9.0		9.8	16.0		12.2	V
J1240+2425	3.8	0.7		2.6	55.7		5.3	F
J1241+3844	3.7			3.6			1.0	H
J1251+4317	7.5	>22		11.4	150.3		430.3	V
J1258+2820	4.8	7.0		14.6	22.2		40.2	F
J1300+4352	5.8			<1.4			883.0	F
J1309+4047	5.2	5.6		5.4	16.5		2.6	H
J1319+4851	5.3	5.7		5.2	2.7		4.0	H
J1321+4406	7.5	4.3		3.8	11.9		51.9	F
J1322+3912	5.2	4.6		4.1	18.0		83.9	V
J1330+5202	6.8			8.8			52.0	F
J1336+4735	4.6	3.0		5.7	2.5		17.6	V
J1352+3603	5.2	4.6		4.3	34.6		55.7	V
J1420+2704	6.8	6.2		6.5	3.8		9.7	H
J1436+4820	5.8	5.1			12.9			H
J1459+3337	16.9	14.6			109.4			V
J1530+2705	9.7	5.7		7.0	106.3		33.4	V
J1547+3518	16.5	15.9		>22*	12.2		10.9	V

Table 4. Continued.

Source (1)	$\nu_{\text{ep1}}$ (2)	$\nu_{\text{ep2}}$ (3)	$\nu_{\text{ep3}}$ (4)	$\nu_{\text{ep4}}$ (5)	$V_a$ (6)	$V_b$ (7)	$V_{c,d}$ (8)	Var. (9)
J1602+2646	12.8	13.0			7.5			H
J1613+4223	4.6		4.3	4.4		5.9	12.4	H
J1616+4632	>22			8.5			119.1	F
J1617+3801	11.6	9.4			1.7			H
J1624+2748	12.0	13.3			9.5			H
J1651+3417	8.6		8.4			9.0		H
J1702+2643	21.5		>22			115.5		F
J1719+4804	9.7	6.0	7.5	4.8	37.6	33.8	472.3	V

In the optically-thin regime, the flux density at a given frequency decreases with time:

$$S_1 = S_0 \left( \frac{t_0 + \Delta t}{t_0} \right)^{-2\delta} \quad (4)$$

where  $\delta$  is the spectral index of the electron energy distribution  $N(E) \propto E^{-\delta}$  that originates the radio emission. It is clear from this relationship that substantial variation in the optically-thick regime can be revealed in case that  $\Delta t$  is a non-negligible fraction of the total source age ( $t_0$ ). In our case,  $\Delta t \sim 8$  years and it can produce detectable flux density variation for sources with  $t_0 \sim 100$  years. Among the sources with some changes in the spectral properties compatible with such a scenario, other 7 sources (J0754+3033, J0955+3335, J1004+4328, J1025+2541, J1052+3355, J1322+3912, and J1547+3518) in addition to J1459+3337 show a spectral and flux density variability that may be explained in terms of source expansion. Although in J1459+3337 there are several indicators supporting this interpretation (Oriente & Dallacasa 2008c), in the case of the other sources mentioned here this assumption is based on the flux density and peak variation on a small time range only. Additional observations spanning a longer time interval, together with information on the pc-scale morphology are necessary in order to reliably constrain the source nature.

## 6 CONCLUSIONS

We presented simultaneous multi-frequency VLA observations of 57 sources from the faint HFP sample, carried out at various epochs. From the comparison of the spectral properties we found that 24 objects (4 galaxies, 11 quasars, and 9 empty fields) preserve their convex spectrum without showing any evidence of flux density variability. Of the remaining sources, 12 objects (2 galaxies, 9 quasars, and 1 empty field), selected on the basis of their convex spectrum in the first epoch by Stanghellini et al. (2009), turned out to show a flat spectrum in one of the subsequent observing epochs. The remaining 21 sources (6 galaxies, 13 quasars, and 2 empty fields) possess high levels of variability, although still displaying a convex spectrum. However, among these variable sources we found that in 8 objects the changes in their spectra are consistent with what expected

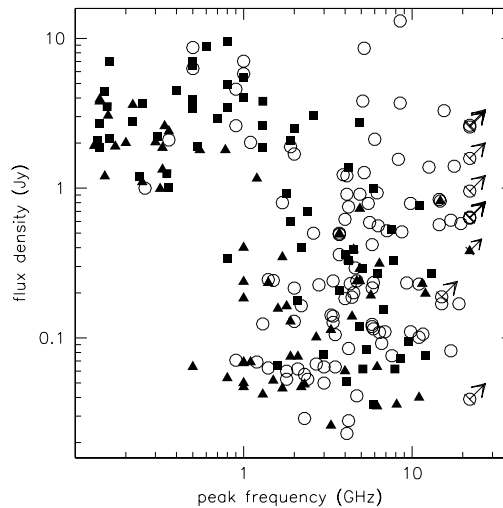


**Figure 5.** The peak frequency versus the peak flux density for the radio sources from the B3-VLA CSS sample (Fanti et al. 2001), the faint GPS sample (Snellen et al. 1998), the half-Jansky GPS sample (Snellen et al. 2002), the GPS sample from Stanghellini et al. (1998), the bright (Dallacasa et al. 2000) and the faint HFP samples (Stanghellini et al. 2009). Circles, squares and triangles refer to quasars, galaxies and empty field, respectively.

if the source is undergoing adiabatically expansion. This implies that out of the 57 sources studied in this paper, 32 objects (56%) can still be considered young radio source candidates. The remaining 25 sources (44%) are part of the flat-spectrum blazar population, indicating that also in samples of faint radio sources, where boosted effects are thought to play a minor role, a large fraction of sources are represented by flaring objects.

The analysis of the optical images of the HFPs hosted by galaxies pointed out the presence of companion galaxies in the target environment, supporting the idea that young radio sources reside in groups. The parent galaxy is usually the brightest elliptical at the group centre with the exception of two sources. In J0804+5431 the galaxy hosting the HFP is at the periphery of the group, and it seems interacting with a close elliptical. A surprising result is represented by the HFP J1109+3831 that is hosted in a

spiral that seems to be interacting with a close elliptical. The fact that young radio sources reside in groups support the idea that the interactions occurring between the galaxies are at the origin of the radio emission.

## ACKNOWLEDGMENTS

We thank S. Bardelli for his help on the analysis of the optical spectra. The VLA and the VLBA are operated by the US National Radio Astronomy Observatory which is a facility of the National Science Foundation operated under cooperative agreement by Associated Universities, Inc. This work has made use of the NASA/IPAC Extragalactic Database NED which is operated by the JPL, Californian Institute of Technology, under contract with the National Aeronautics and Space Administration. Funding for the SDSS and SDSS-II has been provided by the Alfred P. Sloan Foundation, the participating Institutions, the National Science Foundation, the U.S. Department of Energy, the National Aeronautics and Space Administration, the Japanese Monbukagakusho, the Max Planck Society, and the Higher Education Funding Council for England. The SDSS was managed by the Astrophysical Research Consortium for the Participating Institutions.

## REFERENCES

- Abazajian, K.N., Adelman-McCarthy, J.K., Agüeros, M.A., et al., 2009, *ApJS*, 182, 543
- Alberdi, A., Gomez, J.L., Marcaide, J.M., Marsher, A.P., Perez-Torres M.A., 2000, *A&A*, 361, 529
- Bicknell, G.V., Dopita, M.A., O’Dea, C.P., 1997, *ApJ*, 485, 112
- Dallacasa, D., Stanghellini, C., Centonza, M., Fanti, R., 2000, *A&A*, 363, 887
- Edge, A.C., Jones, M., Saunders, R., Pooley, G., Grainge, K., 1996, in *Proceedings of the Second Workshop on GPS and CSS Radio Sources*, ed. I.A.G. Snellen (Leiden: Leiden Observatory), 208
- Fanti, R., Fanti, C., Schilizzi, R.T., Spencer, R.E., Nan Rendong, Parma, P., van Breugel, W.J.M., Venturi, T., 1990, *A&A*, 231, 333
- Fanti, C., Fanti, R., Dallacasa, D., Schilizzi, R.T., Spencer, R.E., Stanghellini, C., 1995, *A&A*, 302, 31
- Fanti, C., Pozzi, F., Dallacasa, D., Fanti, R., Gregorini, L., Stanghellini, C., Vigotti, M., 2001, *A&A*, 369, 380
- Jauncey, D.L., King, E.A., Bignall, H.E., et al., 2003, *PASA*, 20, 151
- Kaiser, C.R., Alexander, P., 1997, *MNRAS*, 286, 215
- O’Dea, C.P., Stanghellini, C., Baum, S.A., Charlot, S., 1996, *ApJ*, 470, 806
- O’Dea, C.P., Baum, S.A., 1997, *AJ*, 113, 148
- O’Dea, C.P., 1998, *PASP*, 110, 493
- Orienti, M., Dallacasa, D., Tinti, S., Stanghellini, C., 2006a, *A&A*, 450, 959
- Orienti, M., Morganti, R., Dallacasa, D., 2006b, *A&A*, 457, 531
- Orienti, M., Dallacasa, D., Stanghellini, C., 2007, *A&A*, 475, 813
- Orienti, M., Dallacasa, D., 2008, *A&A*, 487, 885
- Orienti, M., Dallacasa, D., 2008b, *A&A*, 479, 409
- Orienti, M., Dallacasa, D., 2008c, *A&A*, 477, 807
- Pacholczyk, A.G., 1970, *Radio Astrophysics* (San Francisco: Freeman & Co.)
- Snellen, I.A.G., Bremer, M.N., Schilizzi, R.T., Miley, G.K., van Ojik, R., 1996, *MNRAS*, 279, 1294
- Snellen, I.A.G., Schilizzi, R.T., de Bruyn, A.G., Miley, G.K., Rengelink, R.B., Röttgering, H.J., Bremer, M.N., 1998, *A&AS*, 131, 435
- Snellen, I.A.G., Schilizzi, R.T., Bremer, M.N., Miley, G.K., de Bruyn, A.G., Röttgering, H.J.A., 1999, *MNRAS*, 307, 149
- Snellen, I.A.G., Schilizzi, R.T., Miley, G.K., de Bruyn, A.G., Bremer, M.N., Röttgering, H.J.A., 2000, *MNRAS*, 319, 445
- Snellen, I.A.G., Lehnert, M.D., Bremer, M.N., Schilizzi, R.T., 2002, *MNRAS*, 337, 981
- Stanghellini, C., O’Dea, C.P., Baum, S.A., Laurikainen, E., 1993, *ApJS*, 88, 1
- Stanghellini, C., O’Dea, C.P., Dallacasa, D., Baum, S.A., Fanti, R., Fanti, C., 1998, *A&AS*, 131, 303
- Stanghellini, C., Dallacasa, D., Orienti, M., 2009, *AN*, 330, 223
- TINGAY, S.J., de Kool, M., 2003, *AJ*, 126, 723
- Tinti, S., Dallacasa, D., De Zotti, G., Celotti, A., Stanghellini, C., 2005, *A&A*, 432, 31
- Torniainen, I., Tornikosky, M., Teräsanta, H., Aller, M.F., Aller, H.D., 2005, *A&A*, 435, 839
- Torniainen, I., Tornikoski, M., Lähteenmäki, A., Aller, M.F., Aller, H.D., Mingaliev, M.G., 2007, *A&A*, 469, 451